Ultrasound in Med. & Biol., Vol. 32, No. 1, pp. 73–82, 2006
Copyright © 2006 World Federation for Ultrasound in Medicine & Biology
Printed in the USA. All rights reserved
0301-5629/06/$–see front matter

ELSEVIER

doi:10.1016/j.ultrasmedbio.2005.09.010

● *Original Contribution*

INVESTIGATING PERFLUOROHEXANE PARTICLES WITH HIGH-FREQUENCY ULTRASOUND

Olivier Couture, Peter D. Bevan, Emmanuel Cherin, Kevin Cheung, Peter N. Burns, and F. Stuart Foster

Imaging Research, Sunnybrook Health Sciences Centre, Toronto, ON, Canada

(*Received* 13 *June* 2005, *revised* 25 *August* 2005, *in final form* 1 *September* 2005)

Abstract—Submicron particles filled with liquid perfluorocarbon are currently being studied as a potential ultrasound-targeted contrast agent. The objective of this study was to evaluate the scattering properties of these particles. Sets of perfluorohexane-filled particles of different average sizes (300 nm to 1000 nm) were produced with a constant total volume fraction. The attenuation coefficient was measured in the 15- to 50-MHz frequency range and was found to increase smoothly with frequency and to be independent of the amplitude and bandwidth of the transmitted pulse. The values range from 0.31 to 0.64 dB/mm at 30 MHz for mean particle size ranging from 970 to 310 nm, respectively. The backscattering spectra of the particle solutions were measured and showed no sign of nonlinear scattering. The backscattering coefficient increased with the power 3.9 ± 0.3 of the frequency. These results confirm that liquid perfluorocarbon droplets behave as linear Rayleigh scatterers. (E-mail: olicou@swri.ca) **© 2006 World Federation for Ultrasound in Medicine & Biology.**

Key Words: **Ultrasound, Submicron particles, Perfluorocarbon contrast agent, Attenuation, Scattering.**

INTRODUCTION

High-frequency ultrasound (US), also known as US biomicroscopy (Foster et al. 2000b) is an established tool for *in vivo* imaging of human beings and small animals (Foster et al. 2002). The use of higher frequencies provides near-microscopic resolution for studies of development (Foster et al. 2003), atherosclerosis, tumor growth or angiogenesis (Foster et al. 2000a) and drug effects (Goertz et al. 2002). Because these biologic processes are tied to the molecular microenvironment of the cells, it would be of interest for high-frequency US to go beyond anatomical imaging by allowing the imaging of proteins related to cellular function or dysfunction.

Imaging these proteins is the domain of molecular imaging, where image contrast is determined by the presence of molecular biomarkers, rather than bulk properties of tissue (Weissleder and Mahmood 2001). In the field of high-frequency US, it can be made possible with the use of contrast agents that are attached to specific antibodies or ligands that bind specific receptors on the target cells (Demos et al. 1997; Lanza et al. 1996). These targeted agents have already been used with success in animal models at conventional frequencies (Dayton and Ferrara 2002; Lindner 2002; Villanueva et al. 2004) to highlight the presence of certain molecules related to diseases such as tumor-induced angiogenesis (Ellegala et al. 2003), inflammation (Lindner 2001) atherosclerosis (Villanueva et al. 2002) and thrombi (Schumann et al. 2002).

Of principal importance for targeted imaging is the high echogenicity of US contrast agents at small doses. Contrast agent echogenicity has been optimized at conventional frequencies and extensively discussed in the literature (de Jong et al. 2002, 2000; Dijkmans et al. 2004; Jakobsen 2001; Lindner 2002). However, little work has been done at frequencies higher than 15 MHz. For such an application, two main types of US contrast agents have been described, microbubbles and submicron particles.

Microbubbles are gas encapsulated by lipids, albumin, polymer or surfactants. The contrast caused by microbubbles resides in their inherent acoustic impedance mismatch, their resonant and highly nonlinear behavior and transient behaviors, such as bubble disruption (Correas et al. 2001; de Jong et al. 2002). Their characteristics have been partially studied at high frequency by

Address correspondence to: Olivier Couture, Imaging Research, Sunnybrook Health Sciences Centre, 2075 Bayview Avenue, 6th Floor, S wing, Toronto, ON M4N 3M5 Canada. E-mail: olicou@swri.ca

Morgan et al. (1996). Microbubbles have been used in conjunction with US biomicroscopy by Goertz and colleagues for blood flow measurements (Goertz et al. 2005a, 2005b) and by Deng et al. (1998).

In contrast to microbubbles, submicron particles are filled with liquid perfluorocarbon encapsulated by a lipid shell (Lanza et al. 1996) or fluorosurfactant shell (Couture et al. 2004). Submicron particles have been demonstrated to be useful for targeted imaging at high frequencies (Lanza et al. 1997). Because these particles are reported to be poorly echogenic in the blood (Hughes et al. 2005) but highly echogenic when bound to a target, it may be possible to obtain a high contrast between specific and nonspecific agents. This difference in behavior between bound and unbound particles has been tentatively explained using a transmission line model where the particles were considered to form a layer of perfluorocarbon that acted as a specular reflector (Hall et al. 2000; Lanza et al. 1998; Marsh et al. 2002a, 2002b). However, it has been reported that this transmission line model underestimates the US reflection enhancement of submicron particles attached to a nitrocellulose membrane (Marsh et al. 2002a). This is potentially because of the fact that the particulate nature of the contrast agent is not taken into account. Also, the potential nonlinear behavior, which may arise from a transient vaporization of the liquid perfluorocarbon, are not described or used in this model. To develop a more comprehensive model, the knowledge of the acoustic properties of the particles is critical and requires a thorough investigation.

This paper describes a method to estimate the physical and acoustic properties of submicron perfluorocarbon particles in solution. First, the production of nanoparticles and the dependence of size with respect to the surfactant concentration are described. The acoustic properties include the attenuation and backscattering coefficients of solutions of various sizes of particles at frequencies between 20 and 50 MHz. In particular, potential nonlinear properties of the contrast agent are investigated.

MATERIALS AND METHODS

Particle preparation

The particles were made as simple droplets of perfluorocarbon suspended in water, without consideration for biocompatibility or targeting. Submicron droplets of perfluorocarbon were prepared by combining water, 5% v/v C_6F_{14} (FC72, 3M, St-Paul, MN, USA; boiling point = 56 °C) and 0.07% to 0.8% v/v fluorinated surfactant (Zonyl FSO, Dupont Canada, Mississauga, ON, Canada). A coarse emulsion was obtained by mixing the solution for 1 min with a Vortex mixer. The coarse emulsion was then emulsified continuously in a Microfluidizer (M-110EHI, Microfluidics, Newton, MA, USA) for 3 min at a pressure of 100 MPa. To remove surfactant-stabilized gas bubbles, the solution was centrifuged at 900 *g* for 1 h and the supernatant was removed. Experiments on the remaining solutions were performed in the 48 h after preparation to reduce the effect of size evolution (Oswald ripening). The size of the particles was varied by limiting the surfactant concentration (Vleeschauwer and Meeren 1998).

Particle sizing

The sizes in this study were obtained by dynamic light scattering on a Nanosizer-S (Malvern, Malvern, UK). Measurements were repeated 5 times for each particle population. Because the size distributions obtained with this apparatus (Fig. 1) are weighted by the intensity of the light scattered by the particles, the contribution of bigger particles was overestimated (Hallett et al. 1991). Therefore, in this study, the number distribution was used for a relative comparison of the different populations of submicron particles and not as an absolute measurement of the particle size. It is important to note that, because the total volume fraction of the particles is assumed to be conserved; the number of particles increases as the particles get smaller.

The average size is obtained from the number distribution using the Sauter mean diameter:

$$D = \frac{\sum N_i \delta_i^{\,3}}{\sum N_i \delta_i^{\,2}}, \qquad (1)$$

where N_i is the number of particles of a specific diameter δ_i. The Sauter diameter represents the diameter of a droplet having the same volume:surface ratio as the

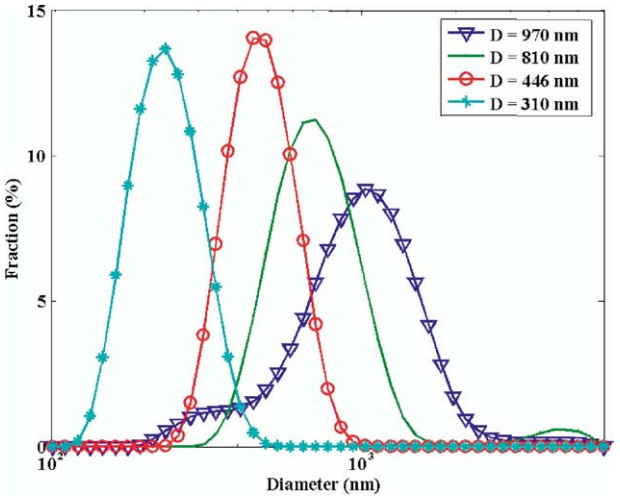

Fig. 1. Intensity-weighted size distribution of four of the particle solutions used in this study.

complete emulsion. When the size of the particle is solely limited by the volume fraction (c_V) and interfacial surface (S), the Sauter D average size is given by (Vleeschauwer et al. 1998):

$$D = \frac{6 \cdot c_v}{S}. \tag{2}$$

Assessment of nonlinearity

Assessment of the nonlinearity of particle scattering was based on previous approaches used to investigate microbubble and nanoparticle US contrast agents. Microbubbles have highly nonlinear resonant scattering properties (Burns 1996; de Jong et al. 2002, 1991) and have been used as a standard. Backscattering spectra of microbubbles show high harmonics, subharmonics (Forsberg et al. 2000) and ultraharmonics that cannot be explained by nonlinear beam propagation. Moreover, the attenuation spectra of microbubbles may peak near the size-dependent resonant frequency of the bubbles (Chen et al. 2002). The attenuation is also amplitude-dependent, unlike linear media. Finally, the attenuation spectrum of microbubbles is also dependent on the length of the pulse sent or, conversely, the bandwidth of the pulses. This study examined the presence of any of these effects for the submicron liquid particles.

Attenuation in solution

A 20-MHz polyvinylidene difluoride (PVDF) transducer (12-mm focal length, 10-mm aperture) was aligned and focused on a quartz reflector inserted in a flow cell (Fig. 2). A diluted solution of particles (0.25% v/v PFH), chosen to reduce the effect of potential multiple scattering, was circulated through the flow cell by gravity. A series of pulses of different frequency, bandwidth (BW) and amplitude were emitted by an arbitrary waveform generator (AWG2020, Tektronix, Beaverton, OR, USA) and amplified by a power amplifier (M3206, AMT, Anaheim, CA, USA). Echoes reflected from the quartz were collected, bandpass filtered from 10 to 70 MHz, amplified by a 40-dB preamplifier (AU-1313, Miteq, Hauppauge, NY, USA) and digitized by an analog to digital board (DP240, Acqiris, Geneva, Switzerland).

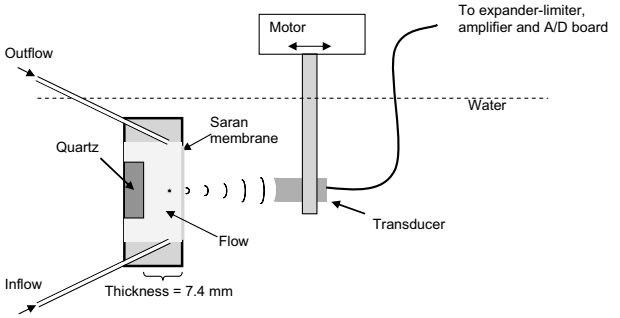

Fig. 2. Setup for attenuation and backscattering experiments. For attenuation experiments, a 20-MHz center frequency transducer (12 mm focal length, f 1.2) is focused on the quartz reflector and, for backscattering, a 50-MHz center frequency transducer (7.5 mm focal length, f 2.5) is focused 2 mm inside the flow cell.

The US attenuation of the solutions relative to water was then calculated from (D'Astous and Foster 1986):

$$\alpha(f) = \frac{-20}{2L}\log_{10}\frac{|A_S(f)|}{|A_W(f)|}\ dB\ \ mm^{-1}, \tag{3}$$

where $A_S(f)$ and $A_W(f)$ are the magnitude spectrum of the reflected signal from the quartz respectively, in the presence and the absence of a sample of thickness L of nanoparticle solution in the propagation path of the US pulse. $A_W(f)$ and $A_S(f)$ were calculated using Matlab (v6.5, Mathworks, Natick, MA, USA). These attenuation measurements were performed using both a set of narrowband pulses (−6-dB, BW 3 MHz) and a broadband pulse (−6-dB, BW 15 MHz). The relative attenuation was calculated in the bandwidth of each pulse using eqn (3), and corrected for the attenuation in water (2.2×10^{-4} dB/mm/MHz^2) (Vogt et al. 2004), to estimate the absolute attenuation in the nanoparticle solution.

Backscattering

The backscattering coefficient was determined from a pulse-echo experiment. This measurement and the required corrections for transducer response, diffraction, frequency-dependent attenuation and frequency-dependent insonification volume were previously described, among others, by Hall et al. (1997); Madsen et al. (1984) and Roberjot et al. (1996). A simpler depth-independent version of the method was used to determine the backscattering coefficient in the focal region:

$$\sigma_{BSC} = \left[\frac{\langle S_m(f,\ F)\rangle}{\langle S_p(f,\ F)\rangle}\right]\left[\frac{1}{0.63^2}\right]\left[\frac{R_p^2 k^2 a^2}{8\pi d\left(1+\left(\frac{ka^2}{4F}\right)^2\right)}\right] \times\left[\frac{4\alpha(f)d\cdot e^{4\alpha(f)\left(-\frac{d}{2}\right)}}{1-e^{4\alpha(f)d}}\right], \tag{4}$$

where $\langle S_m(f,F)\rangle$ is the apparent backscattered power, $\langle S_p(f,F)\rangle$ is the power spectrum of the signal from a reference reflector, R_p is the amplitude reflection coefficient of the reflector, k is the wavenumber, a is the transducer radius, F is the focal length, $\alpha(f)$ is the frequency-dependent attenuation in the solution, d is the length of the gating window (Hamming window in our case) and z is the attenuated path inside the medium.

The first term of eqn (4) is the backscattered power corrected for transducer response. The second term com-

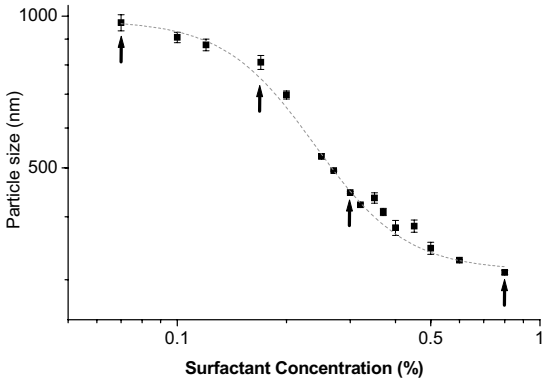

Fig. 3. Average diameter (Sauter diameter D_{32}) of 16 populations of submicron particles obtained by varying the concentration of fluorosurfactant. Arrows = data points used for Fig. 4.

pensates for the loss in energy caused by the gating by a Hamming window. The third term is the correction for the frequency-dependence of the volume of insonification. Finally, the fourth term is the attenuation-correction term.

The apparent backscattered power $\langle S_m(f,F)\rangle$ was measured with a 50-MHz lithium-niobate transducer (7.5-mm focal length, 3-mm aperture) focused 2 mm inside the flow cell (Fig. 2). The set of pulses used for the attenuation measurements was transmitted in the nanoparticle solution and the signal backscattered from the focal region was collected. Backscattered signals were windowed (1 μs mm long Hamming window), Fourier-transformed and the electronic noise was subtracted. In addition to the 16 populations of submicron particles, the experiment was performed on a solution of silica particles (4-μm mean diameter), which was used as a reference linear scatterer (Verbeek et al. 1999). $\langle S_p(f,F)\rangle$ was measured using the reflection of the pulses on a quartz flat positioned in the focal plane of the transducer.

RESULTS

Production of particles

Liquid perfluorocarbon droplets ranging from 300 to 1000 nm were obtained using high-pressure emulsification. As shown in Fig. 1, the intensity-weighted size distribution of the particles is log-normal for smaller particles. The full width-half maximum of the distribution of particles 500 nm in diameter was about 275 nm. For a bigger population of particles, the size distribution was skewed. At lower concentrations of surfactant (< 0.07 %), particles with multiple peaks were obtained.

Note that the particle size will also affect their number because the total volume fraction of particles is kept constant. Smaller particles will be in greater number, which will affect the scattering and the attenuation measurements.

As shown in Fig. 3, the particle size decreased with the amount of surfactant added to the solution. The mean particle diameter as a function of the surfactant concentration followed a sigmoid on a log-log plot. The mean diameter reached a plateau around 1000 nm for the lowest surfactant concentration, and decreased down to another plateau around 300 nm for the highest concentration. The slope in the central part of the sigmoid in Fig. 3 was -0.93 ± 0.03, which is close to the theoretical slope of -1 obtained from eqn (2).

At 72 h after emulsification, an increase in average diameter of up to 50 nm could be observed for the smallest particles. Because the fluorosurfactant used in our preparation tends to create a very bubbly and foamy solution, centrifugation to remove small surfactant-stabilized air bubbles from the solution was a critical step in our particle-production process. Indeed, when small bubbles were not removed from the solution of nanoparticles produced at high concentrations of fluorosurfactant, a significant increase of the backscattering was observed. Centrifugation time and speed were chosen so that most particles were observed to sink to the bottom of the centrifuge tube.

Attenuation

The attenuation curves of 4 of the 16 populations of particles (310, 446, 810 and 970 nm size) obtained using narrowband pulses are shown in Fig. 4. The attenuation increased smoothly with frequency. These curves can be fitted to eqn (5):

$$\alpha(f) = Af^n + B, \tag{5}$$

where α is the frequency-dependent attenuation, f is the frequency and A and B are fitting coefficients. In water, $n = 2$, $A = 2.2 \times 10^{-4}$ (dB/mm/MHz^2) and $B = 0$

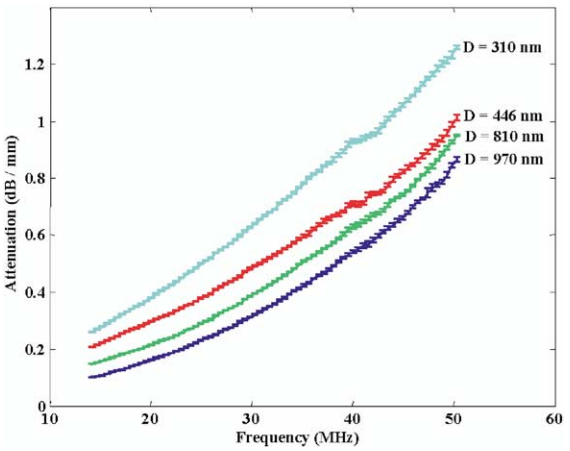

Fig. 4. Narrowband attenuation spectra of C_6F_{14} particles of different diameters; D = Sauter diameter D_{32}.

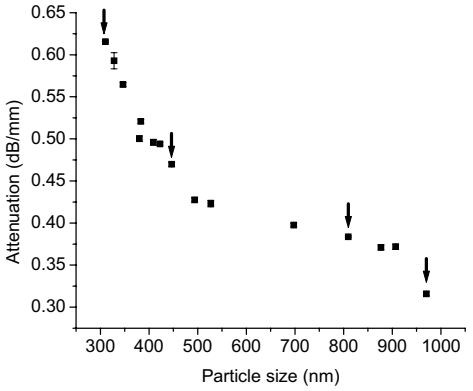

Fig. 5. Absolute attenuation of different populations of submicron particles at 30 MHz. Arrows = data points used for Fig. 4.

(dB/mm) (Vogt et al. 2004). In the solution of submicron particles studied, *n* increased with the particle size from 1.8 to 2.1. However, the overall attenuation decreased with the increasing particle size (Figs. 4 and 5).

Figure 6 shows the attenuation coefficient with respect to particle size at different frequencies. It is normalized because the attenuation increases significantly with frequency. Note that the attenuation started to increase for bigger particles at higher frequencies. This effect became even more pronounced as the frequency increased.

The attenuations in submicron particle solutions obtained using narrowband and broadband pulses are compared in Fig. 7. The attenuations measured using both techniques were identical, within error, for all frequencies, pulses and particle populations. The broadband and narrowband measurements yielded similar results.

Attenuation spectra at two different pressure amplitudes at the focus (300 kPa and 1.8 MPa) were compared

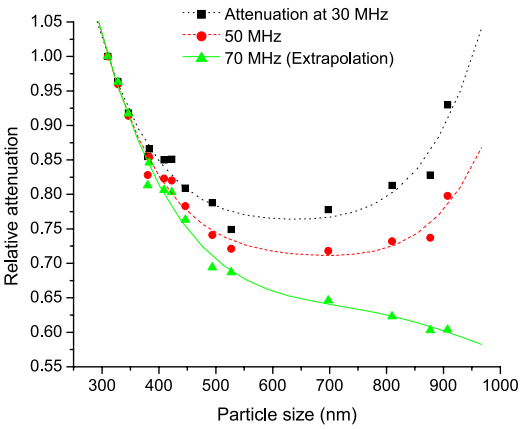

Fig. 6. Relative attenuation of different populations of submicron particles at 30 MHz, 50 MHz and 70 MHz. Errors are smaller than the icons; lines are only visual aids.

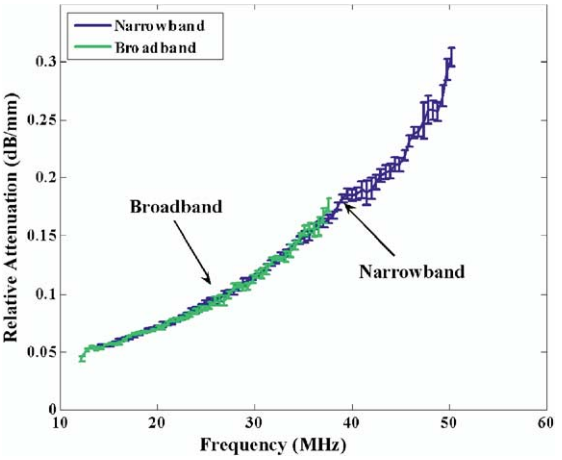

Fig. 7. Comparison of the attenuation obtained with narrowband and broadband pulses (particle size = 970 nm, perfluorocarbon: C_6F_{14}). The usable portion of wideband pulse was shorter than narrowband pulses because of SNR issues.

(Fig. 8) and were found to be independent of the transmitted amplitude.

Backscattering

The backscatter spectra of three different populations of submicron particles and a solution of silica particles insonified with a 34-MHz narrowband pulse are shown in Fig. 9. For these experiments, high transmitted pressures (up to 3.2 MPa) were used because submicron particles do not typically have a high scattering coefficient. The fundamental (at 34 MHz) and the second harmonic (at 68 MHz) were observable in all the samples. No subharmonics or ultraharmonics peaks were detectable. If present, the subharmonic signal was buried in the noise and must be at least 35 dB lower than the

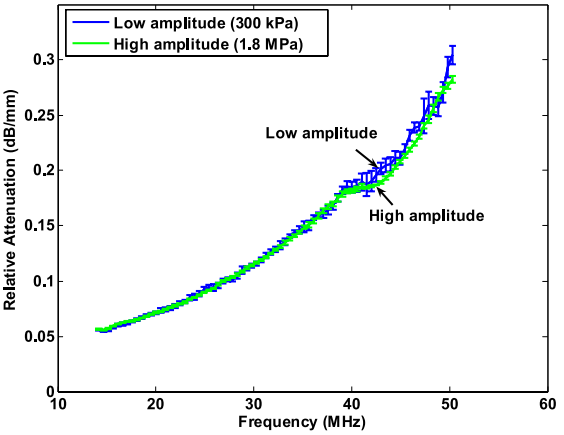

Fig. 8. Comparison of the attenuation obtained at two different pressures (particle diameter = 970 nm, perfluorocarbon: C_6F_{14}).

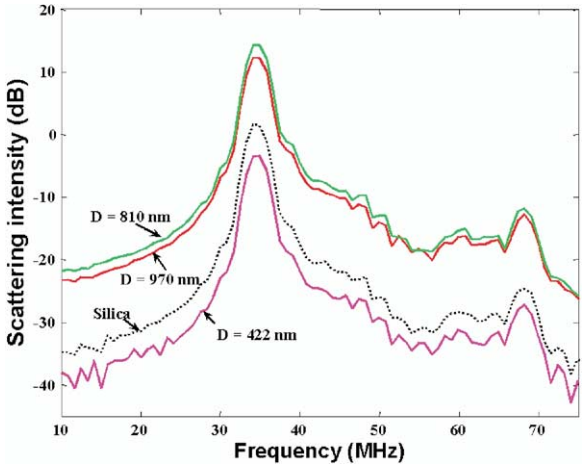

Fig. 9. Backscattering spectra of C_6F_{14} particles of different diameters (D) and silica (33 MHz at 3.2 MPa).

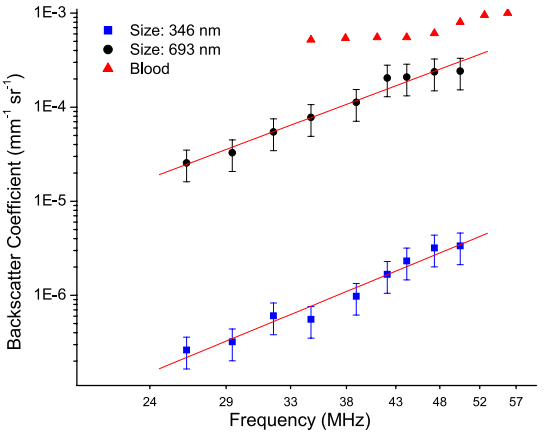

Fig. 11. Backscatter coefficient of two solutions of submicron particles. Slope of the fit for the 693-nm particles is 4.2 ± 0.7 and, for the 346 nm particles, the slope is 3.8 ± 0.2. Average slope for the other samples was 3.9 ± 0.3. Blood data are from Lockwood et al. (1991).

fundamental. In comparison with the level of fundamental, the intensity of the second harmonic was 24 ± 1 dB lower for particles with an average diameter of 920 nm and 810 nm, and 26 ± 1 lower for silica and particles with an average diameter of 422 nm. The difference between the different samples was, thus, not significant, considering the error.

A solution of particles with an average diameter of 530 nm was diluted at different volume fraction of liquid perfluorocarbon relevant to the backscattering experiments (0.03% to 0.375%). The normalized backscattering intensity is plotted in Fig. 10. The relative backscattering increases linearly with the volume fraction of PFH. In preliminary experiments, no clear increase in the relative backscattering intensity could be seen at concentrations beyond 0.375%, which may originate from multiple scattering or the partial correlation of the position of the scatterers.

The increase of the backscattering coefficient with frequency is shown in Fig. 11. The slope of the log-log fit for the larger particle was 4.2 ± 0.7 and, for smaller particles, the slope was 3.8 ± 0.2. The average slope for all samples was 3.9 ± 0.3.

The backscattering coefficients of the 16 populations of particles were also measured. The experimental values are shown in Fig. 12, along with the backscattering coefficients calculated from eqn (4). The error shown was obtained from reproducing the experiment 10 times for the same particle population. Despite a decrease in the number of particles present in the solution, the scattering clearly increased with the size of the particles. On

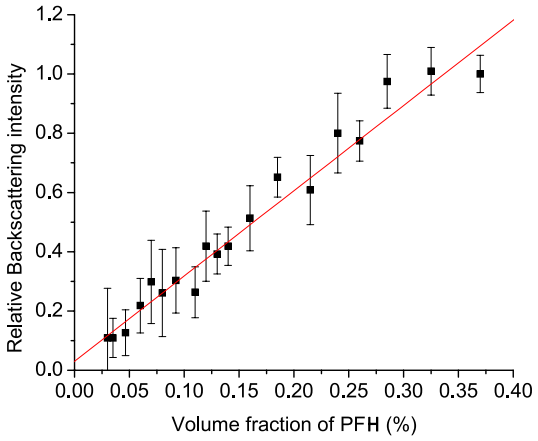

Fig. 10. Normalized backscattering intensity of a solution of submicron particles (diameter ≈ 530 nm) diluted at different concentrations relevant to this experiment.

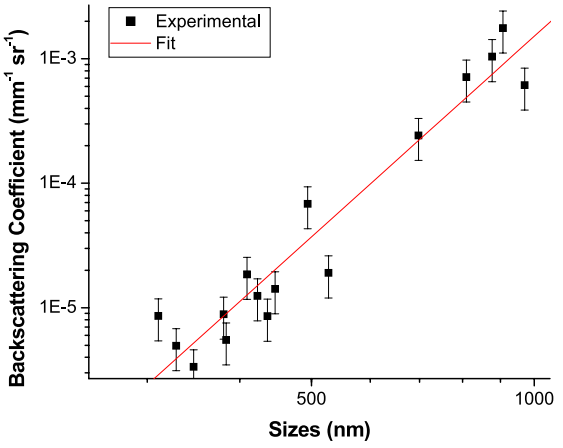

Fig. 12. Backscatter coefficient of different populations of submicron particles at 50 MHz. Slope of the fit is 5.4 ± 0.3.

a log-log plot, a linear fit was obtained with a slope of 5.4 ± 0.3.

DISCUSSION

Production of the particles

The goal of this study was to determine the acoustic behavior of submicron droplets of liquid perfluorocarbon. It was, thus, important to create a reproducible set of populations of particles with, preferably, a narrow size distribution. The fluorosurfactant Zonyl FSO is well-adapted to this purpose. Its aqueous surface tension is low (19 dyn/cm at 0.01% concentration, Dupont), enabling the enclosure of the liquid perfluorocarbon with sufficient stability. Compared to lecithin-stabilized particles (Hughes et al. 2005), the process was simplified by the fact that only three ingredients were used to create the particles and that less surfactant was needed.

The surface covered by the surfactant is linearly proportional to the mass of surfactant added in the solution, assuming it is completely used to coat the particles. Hence, from eqn (2), the Sauter mean diameter of the particles should be inversely proportional to the amount of surfactant. Behavior close to the theoretical prediction is observed in Fig. 3, where the slope of the log-log sigmoid fit was close to −1.

As observed, the size of smaller particles was limited by the amount of energy that was input by the high-pressure emulsifier. More energy is necessary to increase the total interfacial area of the particles. Below 0.07% surfactant concentration, not enough surfactant was present to stabilize the particles.

Linearity of particles

Some contrast agents, such as Echogen, have a boiling point between room temperature and body temperature (Correas and Quay 1996). Consequently, such a contrast agent behaves as a bubble inside the body with its accompanying nonlinear behavior. In this study, we examined whether or not such an effect is observed with droplets of PFH.

PFH was chosen because it has one of the lowest boiling points (56 °C, 3 mol/L) and lowest acoustic impedances (0.875 Mrayl; Marsh et al. 2002a) among usable liquid perfluorocarbons. A low boiling point was supposed to favor nonlinear processes induced by the vaporization of the perfluorocarbon and low acoustic impedance was supposed to enhance the mismatch with the acoustic impedance of the medium (water). The boiling point is still much higher than the temperature at which the study was performed (21 °C). Furthermore, liquid perfluorocarbon enclosed in a droplet has a higher boiling point than the bulk product (Giesecke and Hynynen 2003). However, Kripfgans et al. (2000) showed that droplets of dodecafluoropentane can be vaporized by US and that the threshold of vaporization diminishes with frequency. Giesecke and Hynynen (2003) also observed US-mediated cavitation with PFH droplets at low frequency. If vaporization of the PFH inside the particles studied here were to happen, a nonlinear bubble-like acoustic behavior would be expected.

Attenuation

Several nonlinear phenomena can be observed in the attenuation spectra of bubble solutions. One of the possible observable bubble-like behaviors is a resonance phenomenon in the attenuation spectra. When measurements are performed with narrowband pulses and only the region of the spectra around the fundamental is used to evaluate attenuation, it is expected that a nonlinear behavior would induce a transfer of energy outside the fundamental spectral band. Therefore, a nonlinear effect, either in the propagation or the scattering, or resonance, may lead to increased attenuation at the fundamental, especially when scattering becomes a major contributor at higher frequencies and particle sizes.

In bubble solutions, such as Optison® and Definity®, attenuation decreases with increasing frequency above resonance (Chen et al. 2002). This is quite different from most liquids, such as water, that have an attenuation that increases smoothly with frequency.

Also, the amplitude and the number of cycles of the pulse affect the scattering of microbubbles and, ultimately, their attenuation spectra. The attenuation of gas bubbles augments with the input amplitude with an increase of scattering cross-section because of high harmonic production and from loss caused by damping mechanisms (Chen et al. 2002).

The bandwidth-dependence of the attenuation of bubbles is related to the transient response of the resonant system. It is reflected in a difference of attenuation measured with narrowband and wideband transmitted pulses.

In this study on submicron particle solution, attenuation spectra showed no deviation from a smoothly increasing curve (Fig. 4). Also, the attenuation of submicron droplets was not affected by the bandwidth of the pulses used (Fig. 7). Moreover, increasing the pressure from 300 kPa to 1.8 MPa at focus did not affect the shape of the attenuation curve (Fig. 8). Consequently, based on attenuation measurement, the droplets appear to be acting as linear scatterers in the range of frequency and amplitudes studied.

Backscattering

The backscattering spectra are, themselves, very informative about the acoustic linearity of the submicron

droplets. For example, in high-frequency US, a sign of nonlinear behavior is the appearance of component in the subharmonic frequency range in the backscatter spectrum of microbubbles. The spectrum of submicron particles did not show such a subharmonic content (Fig. 9).

No subharmonics or ultraharmonics could be observed from the scattering spectra of the particles. Second harmonics were detectable in scattering spectra of the particles. However, it has to be noted that very high transmitted pressures (up to 3.2 MPa) were used because submicron particles do not typically have a high scattering coefficient. At high-pressure amplitude, nonlinear propagation does occur in the solution with the consequent generation of harmonics. It is, therefore, important to distinguish the linear scattering of the harmonics generated during nonlinear propagation from the nonlinear scattering itself. To do so, particles of silica that are known to be linear scatterers were used as a reference. Experimentally, the levels of second harmonics caused by PFH particles are equal within error than those from silica particles (Fig. 9). Thus, it can be concluded that, even at high amplitudes, most second harmonics are generated during propagation of the wave through water, and are linearly scattered by the particles.

Rayleigh scattering

The overall scattering of PFH submicron particles increases linearly with concentration (Fig. 10). Such a behavior demonstrates that the measurements are not affected by multiple scattering. From the flow cell design, it can also be assumed that the scattering was completely decorrelated in the focal region of the transducer. Moreover, the previous section also demonstrated that the submicron particles are small (1 micron in comparison to a 30-micron minimum wavelength), linear scatterers and probably remain liquid under the experimental conditions of this study. These results support the hypothesis of Rayleigh scattering to describe the submicron PFH particles. Therefore, the backscattering cross-section (σ_b) for a particle whose volume is equal to the expected volume $E[V_S]$ can be expressed as (Rayleigh 1945):

$$\sigma_b = \left(\frac{k^2 E[V_S]}{4\pi}\right)^2 \left[\frac{\kappa - \kappa_0}{\kappa_0} - \frac{\rho - \rho_0}{\rho_0}\right]^2, \qquad (6)$$

where k is the wave number, V_S is the volume distribution of the scatterers, κ is the compressibility and ρ the density. The subscript *0* refers to the external medium.

Figure 11 shows that the frequency-dependence of the scattering coefficient is within error of the theoretical power of 4 for Rayleigh scattering. It is more difficult to conclude anything from the size-dependence (Fig. 12) because of the variation in the number concentration for each sample and the finite size distribution of the particles.

In this study, the absolute backscattering coefficient at 50 MHz of the submicron particles at 0.25% concentration was determined to be 3×10^{-6} Sr^{-1} mm^{-1} for smaller particles (300 nm) to 2×10^{-3} Sr^{-1} mm^{-1} for bigger particles (900 nm). In comparison, the backscattering coefficient of a fibrous plaque at 50 MHz lies between 0.01 to 0.1 Sr^{-1} mm^{-1} (Machado and Foster 2001) and the backscattering coefficient of blood at 50 MHz is around 0.0005 Sr^{-1} mm^{-1} (Lockwood et al. 1991). Consequently, if the particles of concern were to be perfused, they would probably not significantly increase the blood contrast in high-frequency US.

It is theoretically possible to calculate the expected Rayleigh backscattering coefficient for a distribution of particles (Mo and Cobbold 1986). However, the size distribution has to be known with precision, which is not the case in this study. Furthermore, because of the inherently low backscattering coefficient of the PFH particles, the signal-to-noise ratio was low, especially for smaller particles. Also, because of practical limitations, a limited number of detectable scatterers were studied. Hence, the phase of the signal from the particles is not uniformly distributed and the signal envelope follows a K-distribution rather than a Rayleigh distribution. This deviation decreases for increasing particle size. It was impossible to correct for the phase of the signal because of insufficient statistics.

The issue to find the expected backscattering coefficient highlights the problems related to the measurement of backscattering coefficient for dilute solutions of weak scatterers. Not only are measurements affected by diffraction and attenuation, but they rely also on the decorrelation of the echo signals from the particles, requiring a significant amount of these particles to ensure sufficient backscattered signal averaging. The submicron particles are, themselves, weak scatterers in solution because of their size, but also because of the low mismatch in acoustic impedance with the surrounding water (PFH = 0.875 MRayl vs. water = 1.5 MRayl). The weak scattering of the particles in solution is one of the motivations for their use as targeted contrast agents, but makes their study more challenging.

This study confirms some conclusions about submicron perfluorocarbon particles found in the literature. The apparent backscattering and attenuation of perfluoro-octyl bromide particles in blood was previously measured at frequencies up to 15 MHz (Hughes et al. 2005) at various powers. They also found no evidence of nonlinear phenomena. The particles have also been characterized when bound to a surface (Lanza et al. 1998). Our study was concerned about the attenuation and backscattering coefficients at higher frequencies for PFH particles of various sizes. It also

describes the production of simple droplets and their modeling as Rayleigh scatterers.

The study of the backscattering coefficient of PFH particles was performed for dilute suspensions. However, the particles are intended to be used, not as a blood-pool contrast agent, but as a bound agent. Targeted agents were shown to increase the reflectivity of surfaces significantly, a phenomenon that was modeled previously (Lanza et al. 1998), based on the idea that these particles would form a layer and act as a transmission line. This model is limited because it does not take into account surface roughness, surface density of the particles or their size distribution. It may be possible to develop a model where the particles act as independent scatterers and where their impulse response functions are summed to obtain the total reflectivity enhancement.

Dependence of attenuation on size

It is interesting to note that, although the scattering increased with the size of the particles, the overall attenuation decreased. Such behavior can be understood from the description of attenuation in emulsion given by McClements (1996). Four components are taken into account, intrinsic absorption, thermal absorption, viscoinertial absorption and scattering. The intrinsic absorption depends on the proportion of each phase in the emulsion and is independent of the droplet size. The viscoinertial and thermal components originate from frictional losses during particle oscillation and the asymmetrical heat flow, in and out of the droplets. The content of the droplets determines the size at which the absorption of the solution will be maximal. For Rayleigh scattering, the scattering contribution depends on the fourth power of the frequency and the third power of the particle radius. It becomes the main factor in attenuation for high frequencies or large particles. The curve in Fig. 5 is the summation of the growing scattering and the decay of the viscoinertial and thermal processes. This study suggests that the contribution of the scattering in the attenuation is lower than the contributions from the viscoinertial and the thermal attenuation, which may be understood from the fact that the experiments were performed in a frequency range covering what McClements refers to as "the long wavelength regime and the intermediate wavelength regime." Another clue is that the scattering contribution becomes more evident when the frequency is increased from 30 MHz to 70 MHz (Fig. 6).

CONCLUSIONS

A solution of water, PFH and fluorosurfactant can be used to create a simple model for liquid PFH submicron droplets. Changing the concentration of the fluorosurfactant easily modifies the size of the particles. By varying the concentration in PFH, one can change the concentration in particles. Unlike gas-filled US contrast agents, these submicron particles do not undergo strong resonance or strong nonlinear acoustic behavior. The frequency and size-dependence of the backscattering coefficient of the submicron particles correspond reasonably well to the theory of Rayleigh scattering. For volume concentrations of 0.25%, the backscattering coefficient of the particles is around 0.0002 (Sr^{-1} mm^{-1}) for particles of 700 nm in size. This low value suggests that these particular agents are unlikely to be useful as freely circulating contrast agents at high-frequency US.

Knowing that submicron particles made of liquid PFH are behaving closely to linear Rayleigh scatterers is essential in the modeling of their acoustic behavior attached to a surface. The fact that the increase in signal intensity is caused by acoustic impedance mismatch between the particles and the medium and not because of resonance or vaporization of the liquid perfluorocarbon has been confirmed. Based on these findings, it may be easier to explain the contrast mechanism of the submicron particles and improve the methods for their detection.

Acknowledgements—The authors thank John Cannata for kindly providing an excellent 50-MHz lithium-niobate transducer. They also thank the Canadian Institute of Health Research, the Ontario Challenge Fund and the National Cancer Institute of Canada for their funding.

REFERENCES

Burns PN. Harmonic imaging with ultrasound contrast agents. Clin Radiol 1996;51(Suppl. 1):50–55.

Chen Q, Zagzebski J, Wilson T, Stiles T. Pressure-dependent attenuation in ultrasound contrast agents. Ultrasound Med Biol 2002;28: 1041–1051.

Correas JM, Quay SD. EchoGen emulsion: A new ultrasound contrast agent based on phase shift colloids. Clin Radiol 1996;51(Suppl. 1):11–14.

Correas JM, Bridal L, Lesavre A, et al. Ultrasound contrast agents: Properties, principles of action, tolerance, and artifacts. Eur Radiol 2001;11:1316–1328.

Couture O, Cherin E, Foster FS. Acoustical characterization of submicron particles of perfluorocarbon in solution. Proc. of the IEEE Ultrason Sympos 2004;2:1387–1390.

D'Astous FT, Foster FS. Frequency dependence of ultrasound attenuation and backscatter in breast tissue. Ultrasound Med Biol 1986; 12:795–808.

Dayton PA, Ferrara KW. Targeted imaging using ultrasound. J Magn Reson Imaging 2002;16:362–377.

de Jong N, Bouakaz A, Frinking P. Basic acoustic properties of microbubbles. Echocardiography 2002;19:229–240.

de Jong N, Frinking PJ, Bouakaz A, Ten Cate FJ. Detection procedures of ultrasound contrast agents. Ultrasonics 2000;38:87–92.

de Jong N, Ten Cate FJ, Lancee CT, Roelandt JR, Bom N. Principles and recent developments in ultrasound contrast agents. Ultrasonics 1991;29:324–330.

Demos SM, Onyuksel H, Gilbert J, et al. In vitro targeting of antibody-conjugated echogenic liposomes for site-specific ultrasonic image enhancement. J Pharm Sci 1997;86:167–171.

Deng CX, Lizzi FL, Silverman RH, Ursea R, Coleman DJ. Imaging and spectrum analysis of contrast agents in the in vivo rabbit eye using

very-high-frequency ultrasound. Ultrasound Med Biol 1998;24: 383–394.
Dijkmans PA, Juffermans LJ, Musters RJ, et al. Microbubbles and ultrasound: From diagnosis to therapy. Eur J Echocardiogr 2004; 5:245–256.
Ellegala DB, Leong-Poi H, Carpenter JE, et al. Imaging tumor angiogenesis with contrast ultrasound and microbubbles targeted to alpha(v)beta3. Circulation 2003;108:336–341.
Forsberg F, Shi WT, Goldberg BB. Subharmonic imaging of contrast agents. Ultrasonics 2000;38:93–98.
Foster FS, Burns PN, Simpson DH, et al. Ultrasound for the visualization and quantification of tumor microcirculation. Cancer Metastasis Rev 2000a;19:131–138.
Foster FS, Pavlin CJ, Harasiewicz KA, Christopher DA, Turnbull DH. Advances in ultrasound biomicroscopy. Ultrasound Med Biol 2000b;26:1–27.
Foster FS, Zhang M, Duckett AS, Cucevic V, Pavlin CJ. In vivo imaging of embryonic development in the mouse eye by ultrasound biomicroscopy. Invest Ophthalmol Vis Sci 2003;44:2361–2366.
Foster FS, Zhang MY, Zhou YQ, et al. New ultrasound instrument for *in vivo* microimaging of mice. Ultrasound Med Biol 2002;28:1165–1172.
Giesecke T, Hynynen K. Ultrasound-mediated cavitation thresholds of liquid perfluorocarbon droplets *in vitro*. Ultrasound Med Biol 2003; 29:1359–1365.
Goertz DE, Cherin E, Needles A, et al. High frequency nonlinear B-scan imaging of microbubble contrast agents. IEEE Trans Ultrason Ferroelec Freq Control 2005a;52:65–79.
Goertz DE, Needles A, Burns PN, Foster FS. High-frequency, nonlinear flow imaging of microbubble contrast agents. IEEE Trans Ultrason Ferroelec Freq Control 2005b;52:495–502.
Goertz DE, Yu JL, Kerbel RS, Burns PN, Foster FS. High-frequency Doppler ultrasound monitors the effects of antivascular therapy on tumor blood flow. Cancer Res 2002;62:6371–6375.
Hall CS, Lanza GM, Rose JH, et al. Experimental determination of phase-velocity of perfluorocarbons: Applications to targeted contrast agent. IEEE Trans Ultrason Ferroelec Freq Control 2000;47: 75–83.
Hall CS, Marsh JN, Hughes MS, et al. Broadband measurements of the attenuation coefficient and backscatter coefficient for suspensions: A potential calibration tool. J Acoust Soc Am 1997;101:1162–1171.
Hallett FR, Watton J, Krygsman PH. Vesicle sizing: Number distributions by dynamic light scattering. Biophys J 1991;59:357–362.
Hughes MS, Marsh JN, Hall CS, et al. Acoustic characterization in whole blood and plasma of site-targeted nanoparticle ultrasound contrast agent for molecular imaging. J Acoust Soc Am 2005;117: 964–972.
Jakobsen JA. Ultrasound contrast agents: Clinical applications. Eur Radiol 2001;11:1329–1337.
Kripfgans OD, Fowlkes JB, Miller DL, Eldevik OP, Carson PL. Acoustic droplet vaporization for therapeutic and diagnostic applications. Ultrasound Med Biol 2000;26:1177–1189.
Lanza GM, Trousil RL, Wallace KD, et al. In vitro characterization of a novel, tissue-targeted ultrasonic contrast system with acoustic microscopy. J Acoust Soc Am 1998;104:3665–3672.
Lanza GM, Wallace KD, Fischer SE, et al. High-frequency ultrasonic detection of thrombi with a targeted contrast system. Ultrasound Med Biol 1997;23:863–870.
Lanza GM, Wallace KD, Scott MJ, et al. Novel site-targeted ultrasonic contrast agent with broad biomedical application. Circulation 1996; 94:3334–3340.
Lindner JR. Assessment of inflammation with contrast ultrasound. Prog Cardiovasc Dis 2001;44:111–120.
Lindner JR. Evolving applications for contrast ultrasound. Am J Cardiol 2002;90:72J–80J.
Lockwood GR, Ryan LK, Hunt JW, Foster FS. Measurement of the ultrasonic properties of vascular tissues and blood from 35–65 MHz. Ultrasound Med Biol 1991;17:653–666.
Machado JC, Foster FS. Ultrasonic integrated backscatter coefficient profiling of human coronary arteries in vitro. IEEE Trans Ultrason Ferroelec Freq Control 2001;48:17–27.
Madsen EL, Insana MF, Zagzebski JA. Method of data reduction for accurate determination of acoustic backscatter coefficients. J Acoust Soc Am 1984;76:913–923.
Marsh JN, Hall CS, Scott MJ, et al. Improvements in the ultrasonic contrast of targeted perfluorocarbon nanoparticles using an acoustic transmission line model. IEEE Trans Ultrason Ferroelec Freq Control 2002a;49:29–38.
Marsh JN, Hall CS, Wickline SA, Lanza GM. Temperature dependence of acoustic impedance for specific fluorocarbon liquids. J Acoust Soc Am 2002b;112:2858–2862.
McClements D. Principles of ultrasonic droplet size determination in emulsions. Langmuir 1996;12:3454–3461.
Mo LY, Cobbold RSA. stochastic model of the backscattered Doppler ultrasound from blood. IEEE Trans Biomed Eng 1986;33:20–27.
Morgan K, Dayton P, Klibanov S, et al. Properties of contrast agents insonified at frequencies above 10 MHz. Proc. of the IEEE Ultrason Sympos 1996;2:1127–1130.
Rayleigh JWS. The theory of sound. 2nd ed. New York: Dover, 1945.
Roberjot V, Bridal L, Laugier P, Berger G. Absolute backscatter coefficient over a wide range of frequencies in a tissue-mimicking phantom containing two populations of scatterers. IEEE Trans Ultrason Ferroelec Freq Control 1996;43:970–978.
Schumann PA, Christiansen JP, Quigley RM, et al. Targeted-microbubble binding selectively to GPIIb IIIa receptors of platelet thrombi. Invest Radiol 2002;37:587–593.
Verbeek XA, Willigers JM, Brands PJ, Ledoux LA, Hoeks AP. Measurement of the contrast agent intrinsic and native harmonic response with single transducer pulse waved ultrasound systems. Ann Biomed Eng 1999;27:670–681.
Villanueva FS, Klibanov A, Wagner WR. Microbubble-endothelial cell interactions as a basis for assessing endothelial function. Echocardiography 2002;19:427–438.
Villanueva FS, Wagner WR, Vannan MA, Narula J. Targeted ultrasound imaging using microbubbles. Cardiol Clin 2004;22:283–298.
Vleeschauwer DD, Meeren PVD. A dynamic light scattering study of the influence of the phospholipid concentration in a model perfluorocarbon emulsion. Colloids Surfaces B Biointerfaces 1998;11: 321–329.
Weissleder R, Mahmood U. Molecular imaging. Radiology 2001;219: 316–333.
Vogt M, Paul B, Scharenberg S, Scharenberg R, Ermert H. Analysis and measurement of spectral characteristics and spatial resolution for high frequency ultrasound imaging systems. Proceedings of the IEEE Ultrason Sympos 2004;3:2137–2140.